X-ray Imaging of Stress and Strain of Diamond, Iron, and Tungsten at Megabar Pressures

Russell J. Hemley,* Ho-kwang Mao, Guoyin Shen,†
James Badro, Philippe Gillet, Michael Hanfland,
Daniel Häusermann

Synchrotron x-ray imaging and stress measurements of diamond-anvil cell gaskets revealed large elastic strains at the diamond tip at a pressure of 300 gigapascals. The diamond, generally considered a rigid body, bent 16 degrees over a distance of 300 micrometers without failure. To complement these measurements, a technique was developed that permits x-ray diffraction to be measured through a beryllium gasket. Measurements on tungsten and iron revealed the strain anisotropy, deviatoric stress, and texture and showed that the yield strengths of these materials increase by up to two orders of magnitude at confining pressures of 200 to 300 gigapascals. The results allow identification of the maximum amount of strain accommodated by the anvil tips before failure. Further development of ultrahigh pressure techniques requires relieving stress concentrations associated with this large elastic deformation.

The ability to confine and study materials at pressures in the multimegabar range (>200 GPa) is a result of continued refinements in the diamond-anvil cell (*1*), including the development of the long piston-cylinder megabar cell design (*2*), the introduction of beveled anvils (*3*), the extension of the range of optical (*4*–*6*) and x-ray (*5*–*8*) pressure calibration, the advent of new classes of megabar devices (*9*, *10*), and the development of increasingly sensitive and accurate microanalytical techniques for probing materials under high-pressure conditions (*11*). Despite these advances, however, our knowledge of material behavior under extreme pressures has been limited by a lack of information on the three-dimensional distribution of stress and strain and the ultimate strength of materials under these conditions. Here we report the development and application of techniques that permit imaging and measurement of stress-strain distributions and deformation of materials at multimegabar pressures.

The behavior of materials in highly stressed states can differ considerably from that near ambient conditions. For example, otherwise strong and hard materials can develop texture and plastically deform at megabar pressures (>100 GPa) (*12*–*15*). To date, however, estimates of the stress-strain states and yield strength of materials under these conditions have been inferred from indirect measurements and extrapolation from lower pressure data (*16*–*23*), or from higher pressure experiments using limited stress-strain geometries (*8*, *14*, *24*). In addition to the fundamental interest in these properties (*25*), such information on high-strength materials is crucial for extending the range of static compression techniques to still higher pressures. This extension requires direct determination of the stress-strain distributions of all load-bearing components of the high-pressure device, including elastic deformation of the anvils and elastic and plastic deformation of the gaskets. Elastic deformation of diamond anvils has been inferred from optical observations (*15*) and modeled theoretically (*26*), but it has not been measured directly above 200 GPa (*27*).

Two experiments were carried out with

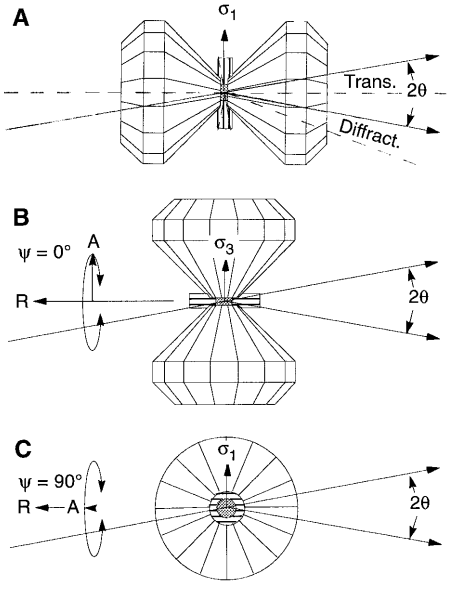

Fig. 1. Three geometries for the diamond-cell x-ray experiments reported here. (**A**) Conventional (axial) geometry for x-ray diffraction and transmission. (**B**) Radial diffraction geometry with $\psi = 0°$ and (**C**) radial diffraction geometry, $\psi = 90°$. A, axial direction; R, radial direction; ψ, angle between the diffraction vector and the load axis; σ_1 and σ_3 are the radial and normal stresses, respectively. In studies of the behavior of gasket material itself at ultrahigh pressures, the gasket is continuous across the tip [that is, the sample chamber is not drilled out (*3*, *5*, *12*)].

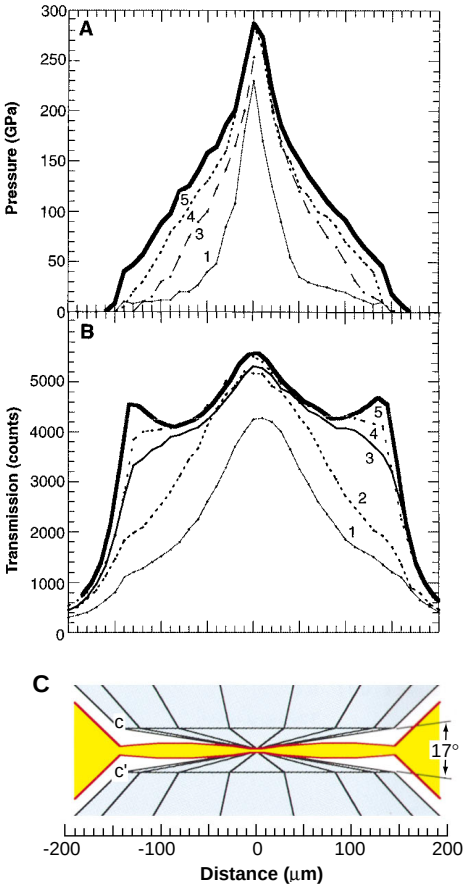

Fig. 2. (**A**) The pressure distribution and (**B**) x-ray transmission profiles as a function of radial distance across (**C**) the diamond culet for the Re-Ta experiment. Each curve gives the distribution at selected loading increments (numbered 1 to 5), where the pressure was determined from x-ray diffraction of Re. (C) shows the original shape of the anvil tips (blue). The dimensions of the central flat, culet, and bevel angles of the two diamonds are 10 μm, 300 μm, and 9°, and 10 μm, 300 μm, and 8°, respectively, giving a total bevel angle of 17°. The yellow region shows the gasket shape at the highest load and the extent of diamond deformation such that the average bevel angle is close to zero. A small grain of Ta (~5 μm) was placed on top of the Re gasket at the center before loading; its diffraction was consistent with that of Re, and it did not contribute measurably to the transmission profile.

R. J. Hemley, H.-k. Mao, G. Shen, Geophysical Laboratory and Center for High Pressure Research, Carnegie Institution of Washington, 5251 Broad Branch Road, NW, Washington, DC 20015, USA.
J. Badro and P. Gillet, Laboratoire de Sciences de la Terre (UMR 5570), Ecole Normale Supérieure de Lyon, 46 Allée d'Italie F-69364 Lyon Cedex 07, France.
M. Hanfland and D. Häusermann, European Synchrotron Radiation Facility, BP 220, 38043 Grenoble, France.

*To whom correspondence should be addressed. E-mail: hemley@gl.ciw.edu
†Present address: Consortium for Advanced Radiation Sources, University of Chicago, Chicago, IL 60637, USA.

diamond-anvil cells modified for improved stability and alignment in the multimegabar pressure range (*10*). First, the strain distribution in gaskets and the elastic deformation of the diamonds were determined by direct imaging of the topography of the diamond-anvil surface in situ to pressure $P \sim 300$ GPa. These observations showed that diamond can accommodate remarkably large strains localized over small areas in the anvil tip. Second, using various diffraction geometries (Fig. 1) together with high-strength but x-ray–transparent gaskets, we directly measured the deviatoric stress of the sample and gasket materials associated with the diamond's large deformations. We used intense and highly collimated synchrotron x-ray beams that permit diffraction and transmission measurements with micrometer-scale spatial resolution in three dimensions within the samples (*28*).

The first set of experiments was carried out to determine the pressure distribution and macroscopic strain of the anvil at ultrahigh pressure using the conventional geometry shown in Fig. 1A. Single-beveled diamond anvils with small central flats of 10 μm were used together with rhenium (Re) gaskets. A small grain of tantalum (Ta) was placed on the central flat, and x-ray diffraction of the Ta and Re were used for pressure determination, on the basis of their shock-wave equations of state (*29*). Initially—that is, at zero pressure—the combined bevel angle was 17°. The central sample thickness was only 3 μm after gasket indentation, whereas the edges of the culets of the two diamonds were separated by 45 μm of Re (cc′ in Fig. 2C). Because the Re gasket highly absorbs x-rays, the magnitude of the transmission at a point measured with the 5 μm by 5 μm x-ray beam gives the thickness of the gasket as determined by plastic flow of the metal and the concomitant elastic deformation of the anvil (Fig. 2B). With increasing load, the 17° combined angle at the anvil tip begins to decrease; that is, the anvil tip begins to flatten. At the highest loads, however, the originally straight slope of the bevel transforms to a cup, with the bevel angle reversed at the edge (c in Fig. 2C). The corresponding pressure distribution obtained from diffraction of the gasket with the same micro x-ray beam initially shows the sharp peaked structure associated with the concentration of pressure at the anvil tip (Fig. 2A). With increasing load, the bevel angle decreases, and the peak broadens as the pressure on the culet edge increases, indicating the gradual loss of the central pressure concentration initially created by the bevel.

Rastering the sample position in two dimensions perpendicular to the x-ray beam provides more detailed information (*30*). With the spatial resolution provided by the small x-ray beam, detailed features of the anvil surface, including the 16 facets of the brilliant cut of the diamond, are apparent (Fig. 3). The image of the diamond tip shows that a large amount of macroscopic strain can be accommodated by the cupped anvil tip. The pressure distribution determined from gasket diffraction (Fig. 3) shows that the pressure falls off rapidly from the central region to the edge of the culet (the rim of the cup) and then decreases smoothly with radial distance from the culet edge. When the bevel collapses [giving a shape essentially like that of the flat culet anvils used in the early lower pressure experiments (*1*, *2*)], the pressure advantage provided by the bevel is consumed, and the capability for further pressure increase at the center is limited. Numerous experiments show that diamond failure results when the cupping reaches a critical value such that the transmission at the rim is about one half of that within the cup.

Complementary information is obtained from x-ray diffraction experiments carried out with radial diffraction geometries (Fig. 1, B and C). With the axially symmetric geometry of the diamond cell, the stress-strain field is defined by the radial and normal stresses σ_1 and σ_3 and their associated strains $\Delta\varepsilon_1$ and $\Delta\varepsilon_3$. The hydrostatic stress component is $\sigma_P = (2\sigma_1 + \sigma_3)/3 = \sigma_1 + t/3$, where t is the differential stress (or uniaxial component) $t = \sigma_3 - \sigma_1$ (*31*). With a conventional geometry, the x-ray beam is nearly coaxial with the load axis, and the diffracted beam is collected at either fixed or variable 2θ angle. This approach measures diffraction planes that do not correspond to the maximum strains in the sample (*32*). In fact, the maximum stress-strain states reached on materials at multimegabar confining pressures are unknown. Although such effects were measured at much lower pressures, they have only been estimated theoretically at multimegabar pressures (*8*). There are no direct measurements because of the limited access to the sample allowed by the conventional geometry. The ideal geometry requires passing the x-rays through the gasket to access the sample. However, typical high-strength gaskets such as Re strongly absorb x-rays and preclude such measurements. To solve this problem, we used x-ray–transparent be-

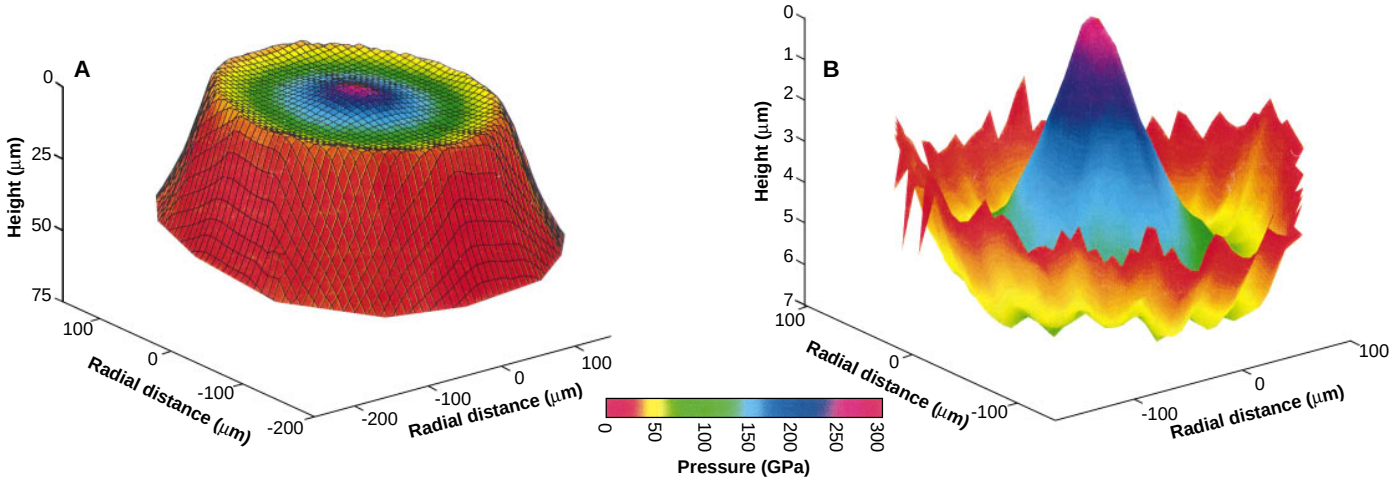

Fig. 3. (**A**) Three-dimensional view of the diamond deformation for the Re-Ta experiment at the highest load (load 5 in Fig. 2A). The Re gasket casts a "mold" to give the deformation at the tips of the two opposed anvils. The horizontal scales show the radial distance from the center of the diamond tips (as in Fig. 2), and the vertical scale is the distance from the tip of an anvil under load for a single diamond. The values correspond to one-half the thickness of the gasket determined from the x-ray transmission and therefore represent the average deformation of the two (symmetrical) opposed anvils. The superimposed colors give the pressure distribution in the gasket measured with the micro x-ray beam at the interface with the diamond. (**B**) Magnified view of the central depression in (A) (the "blue lagoon").

ryllium (Be) gaskets, which permit direct measurements of deviatoric strains at multimegabar pressures.

Polycrystalline W and Fe were loaded in a specially prepared Be gasket (*33*) mounted at the 10-μm tips of single-beveled diamonds. Tungsten remains cubic [body-centered-cubic (bcc) structure] at megabar pressure (*8*), whereas Fe is bcc at low pressure but transforms to the hexagonal closed-packed (hcp) structure at 13 GPa (*13*). The lattice strains were measured in two directions by x-ray diffraction with all three geometries. Diffraction data obtained through the Be gasket (Fig. 4A) show that the relative intensities of diffraction peaks differ drastically between the two directions, indicating a strong preferred orientation under uniaxial deformation. As in previous measurements on ε-Fe with the conventional geometry (*13*), the characteristic 100 and 101 hexagonal reflections were observed, with the 002 reflection nearly absent. The diffraction pattern from the radial x-ray measurement with $\psi = 90°$ is therefore identical to that obtained by axial diffraction (ψ is the angle between the diffraction vector and the load axis). In the radial measurement with $\psi = 0°$, however, the 002 reflection is the strong peak, and the 100 reflection is not observed, indicating alignment of crystallites with the *c* axis, parallel to the load direction (*13*).

The difference in *d*-spacings obtained from the $\psi = 0°$ and $\psi = 90°$ patterns gives the deviatoric strains $F = (d_{0°} - d_{90°})/3d_P$, where $d_P = (d_{0°} + 2d_{90°})/3$ is the *d*-spacing under hydrostatic pressure (*34*). The pressure was determined from the average d_P using the equations of state of W and Fe (*13, 29*). These data can be used to determine the deviatoric stress component *t*, which can be written $t = \sigma_1 - \sigma_3 = 6G\langle F(hkl)\rangle$ (*21*), where G is the aggregate shear modulus and $\langle F(hkl)\rangle$ is the average of *F* over the measured diffraction peaks with indices *hkl*. We find that *t* increases with increasing *P*, reaching values of ~20 GPa for W and Fe at 200 to 300 GPa (Fig. 4B). In Fig. 4B, we also show the stress difference between orientations assuming that the stress is equivalent to the pressure obtained from the equations of state of each material, an approach that significantly overestimates the deviatoric stress (*35*).

The maximum uniaxial stress *t* supported by a material is determined by its strength; that is, $t \leq \sigma_y = 2\tau$, where σ_y and τ are the yield and shear strengths of the material, respectively. It is often assumed in high-pressure experiments that $t = \sigma_y$; however, in general *t* varies with sample environment, and the equality (von Mises condition) holds only if the sample deforms plastically under pressure. Our results indicate that the yield strengths of W and Fe exceed 20 GPa at $P > 200$ to 300 GPa (*36*), a significant increase relative to ambient conditions [where σ_y(W) = 0.6 GPa (*37*) and σ_y(α-Fe) = 0.03 GPa (*38*)]. Moreover, above ~50 GPa, *t* is considerably less than σ_y because diamond cupping arrests the flow of the sample. This difference is confirmed by spatially resolved x-ray diffraction and transmission measurements. Our finding that the yield strengths of W and Fe are higher than the uniaxial stress component is also supported by the theoretical estimates based on scaling to the shear modulus (*25*) and by the extrapolation of Bridgman's data (*39*). Together with our observations for diamond, these results demonstrate that the strength of these materials is dramatically enhanced at ultrahigh pressures.

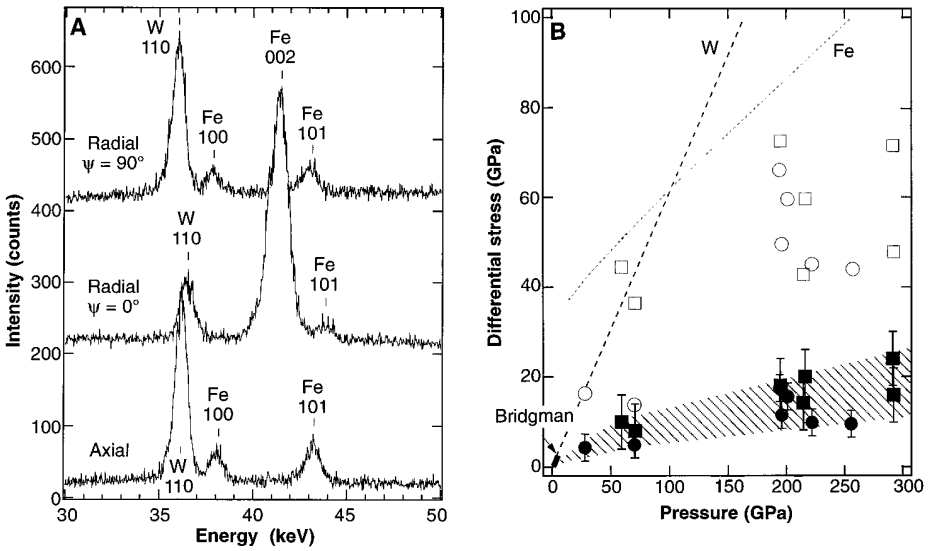

Fig. 4. (**A**) X-ray diffraction patterns measured in the three geometries shown in Fig. 1 at the highest load [σ_P(Fe) = 290 GPa; σ_P(W) = 265 GPa]. (**B**) Differential stress of W (circles) and Fe (squares) as a function of pressure. The solid symbols are the values obtained for *t*; the error bars reflect the experimental error and the uncertainties in shear modulus *G* at high pressure (*40, 41*), and the hatched region reflects the range in measured *t*. The open symbols are the stress differences ($\Delta\sigma$) determined by assuming that the strains measured at $\psi = 0°$ and $\psi = 90°$ correspond to volumetric strains with the stress given by the *P-V* equation of state (*13, 29*). The values of σ_P for the two samples are not the same for the same load because we determine the stress conditions (σ_1, σ_2, and *t*) for each component separately. Bridgman's (*39*) data for the yield strengths σ_y of both materials are shown by the single bold line at low pressures, and the dashed line shows the extrapolation of his data for W. The dashed line for Fe shows an estimate of the theoretical strength for the hcp phase calculated from the scaling $\sigma_y = 2\tau \approx 0.2G$ (*25*), where *G* was determined from recent calculations (*41*).

REFERENCES AND NOTES

1. G. J. Piermarini and C. E. Weir, *J. Res. Natl. Bur. Stand. Sect. A* **66**, 325 (1962); A. Van Valkenburg, in *High Pressure Measurement*, A. Giardini and E. C. Lloyd, Eds. (Butterworths, Washington, DC, 1963), p. 87.
2. H. K. Mao and P. M. Bell, *Science* **191**, 851 (1976); *Carnegie Inst. Washington Yearb.* **77**, 904 (1978).
3. H. K. Mao and P. M. Bell, *Science* **200**, 1145 (1978).
4. G. J. Piermarini, S. Block, J. D. Barnett, R. A. Forman, *J. Appl. Phys.* **46**, 2774 (1975).
5. H. K. Mao, P. M. Bell, J. W. Shaner, D. J. Steinberg, *ibid.* **49**, 3276 (1978); P. M. Bell, J. Xu, H. K. Mao, in *Shock Waves in Condensed Matter*, Y. Gupta, Ed. (Plenum, New York, 1986), p. 125.
6. J. Liu and Y. K. Vohra, *Appl. Phys. Lett.* **64**, 3386 (1994); *J. Appl. Phys.* **79**, 7978 (1996).
7. H. K. Mao *et al.*, *Science* **246**, 649 (1989); *High Pressure Res.* **5**, 773 (1990).
8. A. L. Ruoff, H. Xia, H. Luo, Y. K. Vohra, *Rev. Sci. Instrum.* **61**, 3830 (1990); A. L. Ruoff, H. Xia, Q. Xia, *ibid.* **63**, 4342 (1992).
9. P. Loubeyre *et al.*, *Nature* **383**, 702 (1996).
10. H. K. Mao, R. J. Hemley, A. L. Mao, in *High-Pressure Science and Technology—1993*, S. C. Schmidt *et al.*, Ed. (American Institute of Physics, New York, 1994), p. 1613; H. K. Mao and R. J. Hemley, *High Pressure Res.* **14**, 257 (1996).
11. W. B. Daniels, in *Encyclopedia of Applied Physics*, G. L. Trigg, Ed. (VCH, New York, 1997), vol. 7, p. 495; W. J. Nellis, *ibid.*, vol. 18, p. 541; R. J. Hemley and H. K. Mao, *ibid.*, vol. 18, p. 555.
12. H. K. Mao, P. M. Bell, K. J. Dunn, R. M. Chrenko, R. C. DeVries, *Rev. Sci. Instrum.* **50**, 1002 (1979).
13. H. K. Mao, Y. Wu, L. C. Chen, J. F. Shu, A. P. Jephcoat, *J. Geophys. Res.* **95**, 21737 (1990).
14. R. Jeanloz, B. K. Godwal, C. Meade, *Nature* **349**, 687 (1991).
15. H. K. Mao and R. J. Hemley, *ibid.* **351**, 721 (1991).
16. A. K. Singh and G. C. Kennedy, *J. Appl. Phys.* **45**, 4686 (1974); *ibid.* **47**, 3337 (1976).
17. C.-M. Sung, C. Goetze, H. K. Mao, *Rev. Sci. Instrum.* **48**, 1386 (1977).
18. G. L. Kinsland and W. A. Bassett, *J. Appl. Phys.* **48**, 978 (1977).
19. C. Meade and R. Jeanloz, *J. Geophys. Res.* **93**, 3261 (1988); *ibid.*, p. 3270; *Phys. Rev. B* **42**, 2532 (1990).
20. N. Funamori, T. Yagi, T. Uchida, *J. Appl. Phys.* **75**, 4327 (1994).
21. Y. Meng, D. J. Weidner, Y. Fei, *Geophys. Res. Lett.* **20**, 1147 (1993).
22. D. J. Weidner, Y. Wang, M. T. Vaughan, *Science* **266**, 419 (1994).

23. M. Chai and J. M. Brown, *Geophys. Res. Lett.* **23**, 3539 (1996).
24. T. S. Duffy, R. J. Hemley, H. K. Mao, *Phys. Rev. Lett.* **74**, 1371 (1995).
25. A. Kelly and N. H. Macmillan, *Strong Solids* (Oxford Univ. Press, New York, ed. 3, 1986).
26. W. C. Moss, J. O. Hallquist, R. Reichlin, K. A. Goettel, S. Martin, *Appl. Phys. Lett.* **48**, 1215 (1986).
27. Moreover, because gaskets provide both sample containment and anvil support at high pressures, the gasket material must exhibit ductility as well as high strength under loading (*11*). Yet, most of the properties of relevant materials have not been measured at high loads, nor have the optimum materials and conditions for high-pressure applications necessarily been found.
28. The measurements were carried out at the European Synchrotron Radiation Facility, Grenoble (beam line ID9), using polychromatic x-ray beams collimated to 5 μm by 5 μm at the sample. The primary beam was collimated with three sets of slits, and the diffraction was measured by the energy-dispersive technique with a Ge solid-state detector. All experiments were performed at room temperature. See also (*9*).
29. S. P. Marsh, Ed., *LASL Shock Hugoniot Data* (Univ. of California Press, Berkeley, 1980).
30. The gasket thickness was calculated using Beer's law, $x = (1/\mu)\ \ln(I_0/I)$, where μ is the average (or effective) extinction coefficient for Re at 10 to 60 keV, and I_0 and I are the intensities of the x-rays incident on and transmitted through the gasket. We determined I_0 from measurements at the center of the culet at the maximum load, where the gasket thickness has a minimum (<3 μm), and the effective μ was determined from measurements at the culet edge before diamond deformation, where the thickness was 45 μm. The shape of the tip of each diamond is given by $x/2$. Calibrations at intermediate loads and measurement of plastic deformation of gaskets recovered at zero pressure indicated no measurable effects of pressure on the effective extinction coefficient at these energies.
31. A. K. Singh, *J. Appl. Phys.* **73**, 4278 (1993); A. K. Singh and C. Balasingh, *ibid.* **75**, 4956 (1994).
32. The determination of pressure under nonhydrostatic conditions is valid only for the same geometry in which the calibration was performed. The pressure calibrations involving x-ray diffraction (*6–8*)—including the secondary ruby scale, which is based on diffraction (*5*)—were carried out for the axial geometry. Above 12 GPa and room temperature, all pressure media solidify and therefore exert some degree of nonhydrostatic stress on samples.
33. We prepared the gasket from 1-mm-thick Be metal (Brush Wellman, grade 200) by drilling a conical indentation that matched the shape of the anvil.
34. This quantity is derived from the general expression $d_\psi(hkl) = d_P(hkl)[1 + (1 - 3\cos^2\psi)F(hkl)]$, where ψ is as defined in Fig. 1 (*31*).
35. For example, by this method a stress of 340 GPa is found at the highest load for ε-Fe with $\psi = 0°$, whereas the strain measured for $\psi = 90°$ corresponds to a stress of 290 GPa. This approximation overestimates the deviatoric stress because it neglects the effect of the shear modulus on the measured differential strains (*20, 21*).
36. The results may be compared with the increase in shear strength of Re to 15 GPa at P = 120 GPa (*14*), obtained from the pressure-gradient method (*17*). In this approach, the shear stress is determined from measurement of pressure gradients by $\tau = (h/2)dP(r)/dr$, where h is the sample thickness. As pointed out in (*14, 17, 19*), this analysis depends critically on the shape of the diamond and is only valid when the diamonds remain flat (no cupping) and the sample continues to flow under loading.
37. P. L. Raffo, *J. Less Common Met.* **17**, 133 (1969).
38. W. A. Spitzig and W. C. Leslie, *Acta Metall.* **19**, 1143 (1971).
39. P. W. Bridgman, *Phys. Rev.* **48**, 825 (1935); *Proc. Am. Acad. Arts Sci.* **72**, 45 (1937). Bridgman found that for W and Fe, σ_y increases monotonically to 2.4 and 2.0 GPa, respectively, at confining pressures of 5.0 and 4.2 GPa, respectively.
40. K. W. Katahara, M. H. Manghnani, E. S. Fisher, *J. Phys. F* **9**, 773 (1979); M. W. Guinan and D. N. Beshars, *J. Phys. Chem. Solids* **29**, 541 (1968).
41. P. Söderlind, J. A. Moriarty, J. M. Wills, *Phys. Rev. B* **53**, 14063 (1996); R. E. Cohen, L. Stixrude, E. Wasserman, in preparation.
42. We are grateful to A. K. Singh for many useful discussions and to J. Shu for experimental help. We also thank C. Meade and two anonymous reviewers for comments that improved the manuscript. This work was supported by NSF.

4 February 1997; accepted 28 March 1997

Silicon and Oxygen Self-Diffusivities in Silicate Liquids Measured to 15 Gigapascals and 2800 Kelvin

Brent T. Poe,* Paul F. McMillan, David C. Rubie, Sumit Chakraborty, Jeff Yarger, Jason Diefenbacher

Mass transport properties of silicate liquids exhibit complex behavior as a function of pressure, as the tetrahedral framework structure of the liquid shifts to a more compact arrangement of atoms. For highly polymerized aluminosilicate liquids, oxygen diffusivities pass through a maximum at pressures below 10 gigapascals, whereas up to 15 gigapascals diffusivities continue to increase for sodium tetrasilicate liquid. A diffusivity maximum indicates a change in the mechanism of formation of 5-coordinated silicon or aluminum in the liquid. In the case of aluminosilicate liquids, this mechanism is restricted to aluminum sites in the network, suggesting that not only degree of polymerization, but also the ratio of aluminum to aluminum plus silicon strongly influences the behavior of magmatic processes at depth.

The ascent and emplacement of magma within Earth's crust and mantle are largely controlled by the viscosity and density of silicate melts at high pressure (*1, 2*). Recent studies have shown that viscous flow in high silica liquids is determined by O^{2-} transfer reactions, involving the formation of SiO_5 or AlO_5 intermediate species (*3–5*). These high-coordinate species are also formed during compression of melt (*4–9*), which could explain the reduced viscosity reported for some silicic magmas at pressures extending up to 3 GPa, corresponding to depths of less than 100 km. We have obtained data on the diffusivities of the network-forming ions O^{2-} and Si^{4+} in silicate and aluminosilicate melts at pressures up to 15 GPa, and we use the data to estimate melt viscosity throughout the pressure range of the upper mantle to the transition zone.

Direct viscosity determinations on aluminosilicate melts had been limited to pressures less than 3 GPa (*10–13*). At higher pressures (*14–16*), one can estimate melt viscosity (η) by measuring the O^{2-} diffusivity ($D_{O^{2-}}$) through the Eyring equation,

$$\eta = \frac{k_B T}{D_{O^{2-}} \lambda} \qquad (1)$$

where k_B is the Boltzmann constant (1.38×10^{-23} J K^{-1}), T is absolute temperature, and λ is the "jump" distance of the diffusing ion, taken to be 2.8 Å for O^{2-} (*17*).

The properties of molten aluminosilicates depend on the degree of polymerization of their tetrahedral framework, which is conveniently expressed in terms of the average number of nonbridging O atoms (NBOs) per tetrahedrally coordinated network-forming cation (usually T = Si^{4+} or Al^{3+} and is defined for the liquid at ambient pressure) (*2, 18*). This parameter (NBO/T) varies from zero (fully polymerized) to four, if all Si and Al atoms are tetrahedrally coordinated to O. We focused on (i) a fully polymerized aluminosilicate liquid with a composition of $NaAlSi_3O_8$ (NBO/T = 0), (ii) a partially depolymerized aluminosilicate liquid, $Na_3AlSi_7O_{17}$ (NBO/T = 0.25), and (iii) a further depolymerized Al-free silicate liquid, $Na_2Si_4O_9$ (NBO/T = 0.5).

For all the liquids, O^{2-} diffusivity increased with increasing pressure (Fig. 1), at least initially, as predicted from molecular dynamics (MD) simulations (*19–23*) and consistent with the results of other experimental studies of polymerized silicate liquids (*14–16*). Only the $Na_2Si_4O_9$ samples were ^{30}Si-enriched, and Si^{4+} diffusivities were very similar to those for O^{2-}, also increasing as a function of pressure (Fig. 1).

B. T. Poe and D. C. Rubie, Bayerisches Geoinstitut, Universität Bayreuth, D-95440 Bayreuth, Germany.
P. F. McMillan, J. Yarger, J. Diefenbacher, Department of Chemistry and Biochemistry, Arizona State University, Tempe, AZ 85287, USA.
S. Chakraborty, Mineralogisch-Petrographisches Institut, Universität Köln, D-50674 Köln, Germany.
*To whom correspondence should be addressed. E-mail: Brent.Poe@uni-bayreuth.de